Trajectory Correction Capability Modeling of the Guided Projectiles with Impulse Thrusters

Min Gao, Yongwei Zhang, Suochang Yang, Dan Fang

***Abstract*—A 6-DOF trajectory model with lateral force is established for guided projectiles with impulse thrusters. The trajectory correction capability is simulated under conditions of different impulse shapes, max lateral forces, impulse durations and total impulses of impulse thrusters. As the simulations indicated, the trajectory correction capability has a linear relationship with the total impulse deployed and steadily increases with the total impulse, but has little relationship with impulse shapes, max lateral forces, or impulse durations. However, the actual trajectory correction capability is degraded because projectiles spin and thrusters act with a short-time delay and a certain duration. The function is formulated between the trajectory capability and the impulse duration, projectile spin rate, and impulse action delay. Live firing experiments indicate that the simulations and formulations are effective for engineering design of trajectory correction projectiles with impulse thrusters.**

***Index Terms*—Guided projectiles, impulse thrusters, modeling, trajectory correction capability**

I. Introduction

ARTILLERY rockets are used in the battlefield for indirect fire on distant targets, they have large impact point dispersion and are commonly used as area rather than precision weapons. Modern warfare, however, demands higher precision in order to avoid or reduce the collateral damage as much as possible. One solution for artillery rockets that could meet the demands of modern warfare is to retrofit these projectiles with some level of low cost precision.

Impulse thrusters are a practical low-cost way to correct the flight trajectory of projectiles and improve the firing precision of projectiles.

Research and development on the use of impulse thrusters in order to improve the precision of missiles and rockets has been going on for decades now. The thrusters' application on rockets has been originally considered by Harkins and Brown. They have proposed a method using a set of thrusters to marginalize the off-axis angular rates of the rockets just after exiting the launcher and managed to reduce the impact point dispersion by the factor of 4 [1]. Thanat Jitpraphai and Mark Costello have conducted studies that consider the effect of the number of pulse jets, pulse jet impulse, and trajectory tracking window size on impact point dispersion [2]. S.K.Guta et al. have conducted simulation studies to arrive at tuning parameters, namely the tracking error window size, the required elapsed time between the pulsejet firings and the angle of tolerance between the tracking error and the individual pulsejet force, to get the best trajectory correction performance [3]. D.Corriveau, C.Berner, and V.Fleck have researched the method to determine the impulse thrusters' configurations that yield the best control authority and thus the greatest amount of correction on the projectile trajectory, results indicated that locating the impulse thruster at or aft of the center of gravity provides greater drift correction for a given impulse magnitude [4]. D. Corriveau, P. Wey, and C. Berner have presented a technique to properly pair impulse thrusters on fin-stabilized projectile in order to maximized drift correction while minimizing the range lost due to the angular motion [5]. Recently, Bojan Pavković and Miloš Pavić have presented a simplified control scheme for artillery rockets named the active damping method which performs a correction of disturbances immediately after a rocket exits a launcher tube, the overall performances of the active damping control system in relation to its energy resources – number and magnitude of the pulsejets were analyzed in this paper [6].

Researches on the use of impulse thrusters described above did not involve the impact of impulse shapes and many parameters such as the impulse duration, projectile spin rate, and impulse action delay on the trajectory correction performance. The objective of this paper is to elucidate the impact of the impulse shapes and thruster parameters on the trajectory correction performance for fin-stabilized projectiles though simulations and analyses.

II. Modeling and Methodology

The numerical simulation employed in this study consists of a rigid body six degree of freedom model typically utilized in flight dynamic modeling of projectiles. The general model is illustrated in Fig. 1, in this Figure, l is the axial location of the thruster ring, θ is the phase angle of the impulse force. We established the 6-DOF trajectory model with lateral force by substituting the lateral force and its moment into the ballistic motion equations [7].

Manuscript received July 11, 2015; revised September 29, 2015.

Min Gao is with Electronic Engineering Department, Shijiazhuang Mechanical Engineering College, No.97 Heping West Road, Shijiazhuang, Hebei, 050003, China. (e-mail: gaomin1103@yeah.net).

Yongwei Zhang is with Electronic Engineering Department, Shijiazhuang Mechanical Engineering College, No.97 Heping West Road, Shijiazhuang, Hebei, 050003, China. (corresponding author, phone: 18911136093, e-mail: yongwei1112@sina.com).

Suochang Yang is with Electronic Engineering Department, Shijiazhuang Mechanical Engineering College, No.97 Heping West Road, Shijiazhuang, Hebei, 050003, China. (e-mail: yangsuochang_jx@sina.com).

Dan Fang is with Electronic Engineering Department, Shijiazhuang Mechanical Engineering College, No.97 Heping West Road, Shijiazhuang, Hebei, 050003, China. (e-mail: fangdan1979_jx@sina.com).

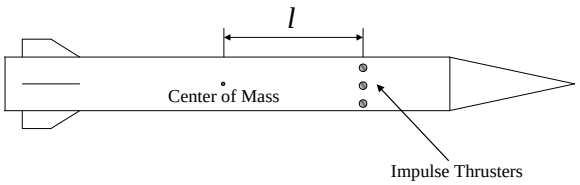

a) Layout of impulse thrusters

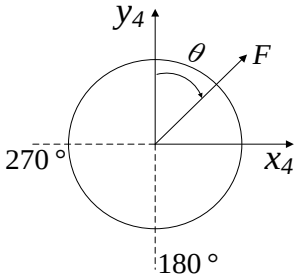

b) Lateral force

Fig. 1. Layout and lateral force of impulse thrusters

The lateral force in quasi-body reference frame is described as

$$\begin{bmatrix} T_{x_4} \\ T_{y_4} \\ T_{z_4} \end{bmatrix} = \begin{bmatrix} 0 \\ T\cos\theta \\ T\sin\theta \end{bmatrix} \tag{1}$$

where T denotes the lateral force of an impulse thruster, θ is the phase angle of the lateral force.

We can get the lateral force in the aero-ballistic reference using the expression

$$\begin{bmatrix} T_{x_2} \\ T_{y_2} \\ T_{z_2} \end{bmatrix} = \begin{bmatrix} \cos\alpha\cos\beta & -\sin\alpha\cos\beta & \sin\beta \\ \sin\alpha & \cos\alpha & 0 \\ -\cos\alpha\sin\beta & \sin\alpha\sin\beta & \cos\beta \end{bmatrix} \begin{bmatrix} T_{x_4} \\ T_{y_4} \\ T_{z_4} \end{bmatrix} \tag{2}$$

where β is the sideslip angle , and α is the attack angle.

The translational kinetic differential equations of the rocket in aero-ballistic reference frame are given by

$$\begin{cases} \dfrac{dV}{dt} = P_{x_2} + F_{x_2} + T_{x_2} \\ V\dfrac{d\theta'}{dt} = P_{y_2} + F_{y_2} + T_{y_2} \\ -V\cos\theta'\dfrac{d\psi_v}{dt} = P_{z_2} + F_{z_2} + T_{z_2} \end{cases} \tag{3}$$

The applied loads appearing in (3) consist of lateral thruster force (T), main rocket thrust (P), and other force (F) components. V , θ' , and ψ_v are the velocity, trajectory incline angle, and flight path azimuth angle of the rocket, respectively.

Lateral moments of an impulse thruster in quasi-body reference frame are given by

$$\begin{bmatrix} M_{Tx_4} \\ M_{Ty_4} \\ M_{Tz_4} \end{bmatrix} = \begin{bmatrix} 0 \\ -T_{z_4} l \\ T_{y_4} l \end{bmatrix} \tag{4}$$

The rotational kinetic differential equations of the rocket in quasi-body reference frame are given by

$$\begin{bmatrix} J_{x_4}\dfrac{d\omega_{x_4}}{dt} \\ J_{y_4}\dfrac{d\omega_{y_4}}{dt} \\ J_{z_4}\dfrac{d\omega_{z_4}}{dt} \end{bmatrix} = \begin{bmatrix} M_{x_4} + M_{Tx_4} \\ M_{y_4} + M_{Ty_4} \\ M_{z_4} + M_{Tz_4} \end{bmatrix} - \begin{bmatrix} 0 \\ \left(J_{x_4} - J_{z_4}\right)\omega_{x_4}\omega_{z_4} \\ \left(J_{y_4} - J_{x_4}\right)\omega_{x_4}\omega_{y_4} \end{bmatrix} + \begin{bmatrix} 0 \\ -J_{z_4}\omega_{z_4}\dfrac{d\gamma}{dt} \\ J_{y_4}\omega_{y_4}\dfrac{d\gamma}{dt} \end{bmatrix} \tag{5}$$

The applied moments appearing in (5) contain contributions from lateral thruster forces (denoted by M_T) and other forces (denoted by M). γ is the Euler roll angle of the rocket. $w_{x_4}, w_{y_4}, w_{z_4}$ are components of the angular rate vector. $J_{x_4}, J_{y_4}, J_{z_4}$ are components of the transverse moment of inertia.

The translational kinematics differential equations of the rocket in inertial frame are given by

$$\begin{cases} \dfrac{dx}{dt} = V\cos\theta'\cos\psi_V \\ \dfrac{dy}{dt} = V\sin\theta' \\ \dfrac{dz}{dt} = -V\cos\theta'\sin\psi_V \end{cases} \tag{6}$$

where x , y , and z are the position vector components of the rocket.

The rotational kinematics differential equations of the rocket in inertial frame are given by

$$\begin{cases} \dfrac{d\vartheta}{dt} = w_{z_4} \\ \dfrac{d\psi}{dt} = \dfrac{1}{\cos\vartheta}w_{y_4} \\ \dfrac{d\gamma}{dt} = w_{x_4} - w_{y_4}\tan\vartheta \end{cases} \tag{7}$$

where ψ and ϑ are the yaw and pitch angle of the rocket, respectively.

The angles in (1) ~ (7) have the relation as follows:

$$\begin{cases} \beta = \arcsin\left[\cos\theta'\sin\left(\psi - \psi_v\right)\right] \\ \alpha = \vartheta - \arcsin\left(\dfrac{\sin\theta'}{\cos\beta}\right) \\ \gamma_v = \arcsin\left(\tan\theta'\tan\beta\right) \end{cases} \tag{8}$$

Equations (1) ~ (8) constitute the 6-DOF trajectory model for guided projectiles with impulse thrusters, they can be solved by the fourth order Runge-Kutta method.

Three impulse shapes are modeled, including the rectangular impulse, triangular impulse, and trapezoidal impulse, as shown in Fig. 2. In Fig. 2, F_m is the max lateral force, t_p is the impulse duration.

The impulse force of the rectangular impulse is described as

$$F = F_m \quad 0 \le t \le t_p \tag{9}$$

The impulse force of the triangular impulse is described as

$$F = \begin{cases} F_m\dfrac{t}{\tau_1} & 0 \le t \le \tau_1 \\ F_m[1 - \dfrac{(t-\tau_1)}{\tau_2}] & \tau_1 < t \le t_p \end{cases} \tag{10}$$

The impulse force of the trapezoidal impulse is described as

$$F=\begin{cases} F_m\dfrac{t}{\tau_1} & 0\le t<\tau_1 \\ F_m & \tau_1\le t<\tau_1+\tau_2 \\ \dfrac{F_m}{\tau_3}(t_p-t) & \tau_1+\tau_2\le t\le t_p \end{cases} \quad (11)$$

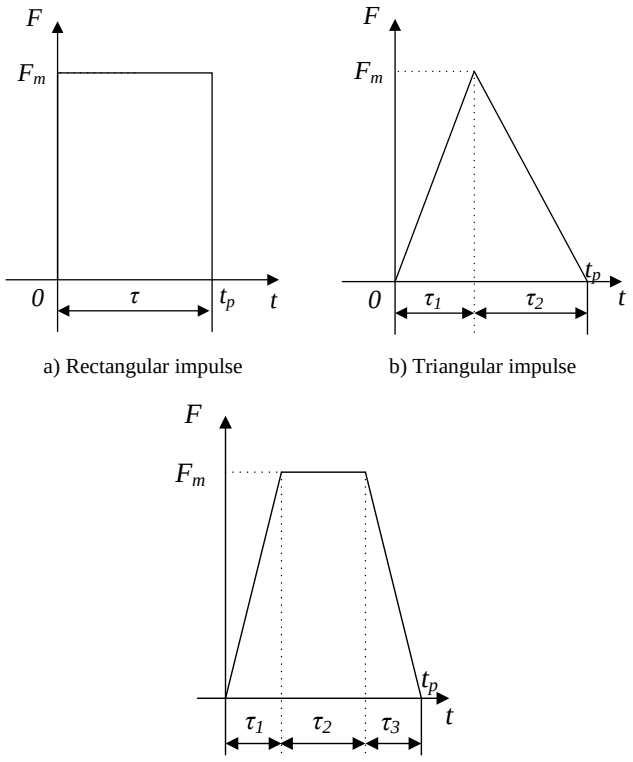

a) Rectangular impulse b) Triangular impulse

c) Trapezoidal impulse

Fig. 2. Impulse shapes

III. Trajectory Correction Capability Simulations

A fin-stabilized, indirect-fire rocket was selected for this study and the results are typical for this class of projectile. The rocket configuration used in the simulation study is a representative 122 mm artillery rocket, 2.99 m long, fin-stabilized. The main rocket motor burns for 3.6 s and imparts an impulse to the rocket of 60788 Ns. During the main rocket motor burns, the forward velocity of the rocket is increased from 39.6 m/s to 958.0 m/s. The rocket weight, mass center location from the nose tip, roll inertia, and pitch inertia before and after burn is 66.1/43.0 kg, 1.43/1.21 m, 0.16/0.12 kg-m2, and 48.42/36.36 kg-m2, respectively. The rocket is launched at sea level toward a target on the ground with altitude and cross range equal zero at a range of 30 km. The simulations have been done using a fourth order Runge-Kutta algorithm. The thruster ring is assumed to be located at 0.869 m from the nose tip of the rocket, and contains a certain number of individual thrusters where each individual thruster imparts an impulse on the rocket body over a certain duration.

The calculation method of trajectory correction capability is: all the individual thrusters are fired for range or cross range correction, the cross range correction capability is obtained through the cross range of the controlled trajectory minus the cross range of the uncontrolled trajectory, and the range correction capability is obtained through the range of the controlled trajectory minus the range of the uncontrolled trajectory. The range correction performance of 10 individual thrusters is shown in Fig. 3, and the cross range performance of 10 individual thrusters is shown in Fig. 4. Each individual thruster has an impulse of 60 Ns, and is fired around 45 s with the firing interval equals 0.2 s. The range correction capability of 10 individual thrusters is 410.0 m, while the cross range correction capability is 561.1 m, according to the calculation method described above.

The trajectory correction capability is simulated under conditions of different impulse shapes, different max lateral forces, different impulse durations, and different total impulses. In these simulations, 10 individual thrusters with rectangular impulse, triangular impulse, or trapezoidal impulse were fired around 45 s with the firing interval equals 0.2 s for range or cross range correction, and the individual thruster impulse was examined over a range of 6 Ns to 60 Ns in steps of 6 Ns. The impulse duration is set as 5 ms, 10 ms, and 20 ms, τ_1、τ_2 obeys the relation $\tau_1=\tau_2$ for the triangular impulse, τ_1、τ_2、τ_3 obeys the relation $2\tau_1=\tau_2=2\tau_3$ for the trapezoidal impulse. The max lateral force of the impulse thrusters is adjusted according to the change of the thruster impulse and the impulse duration. The projectile spin rate was set as 0 r/s to isolate the impact of the projectile spin rate on the trajectory correction performance. Simulation Results is shown in Fig. 5.

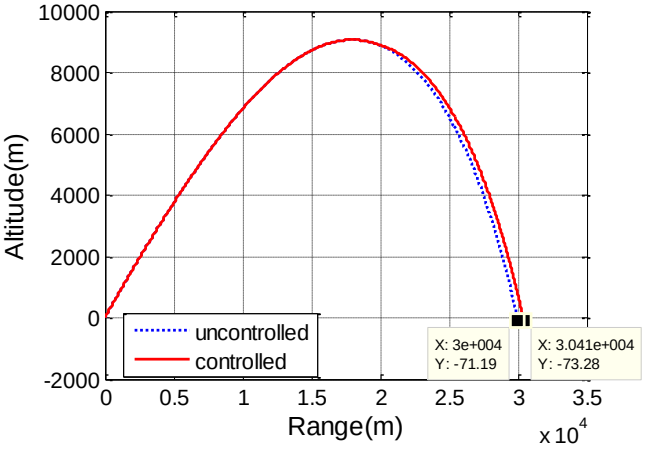

Fig. 3. Range correction performance of thrusters

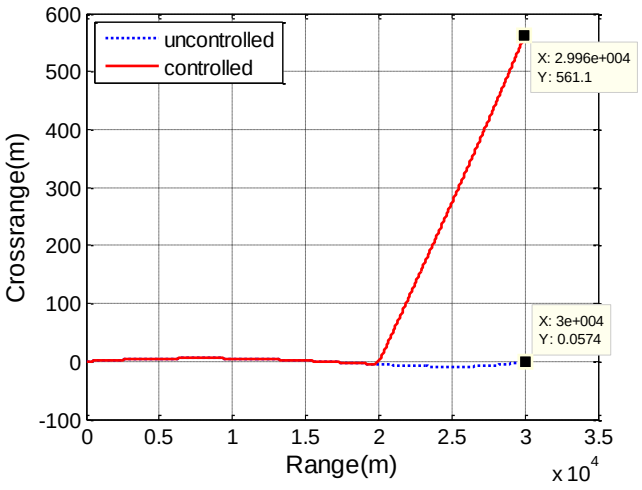

Fig. 4. Cross range correction performance of thrusters

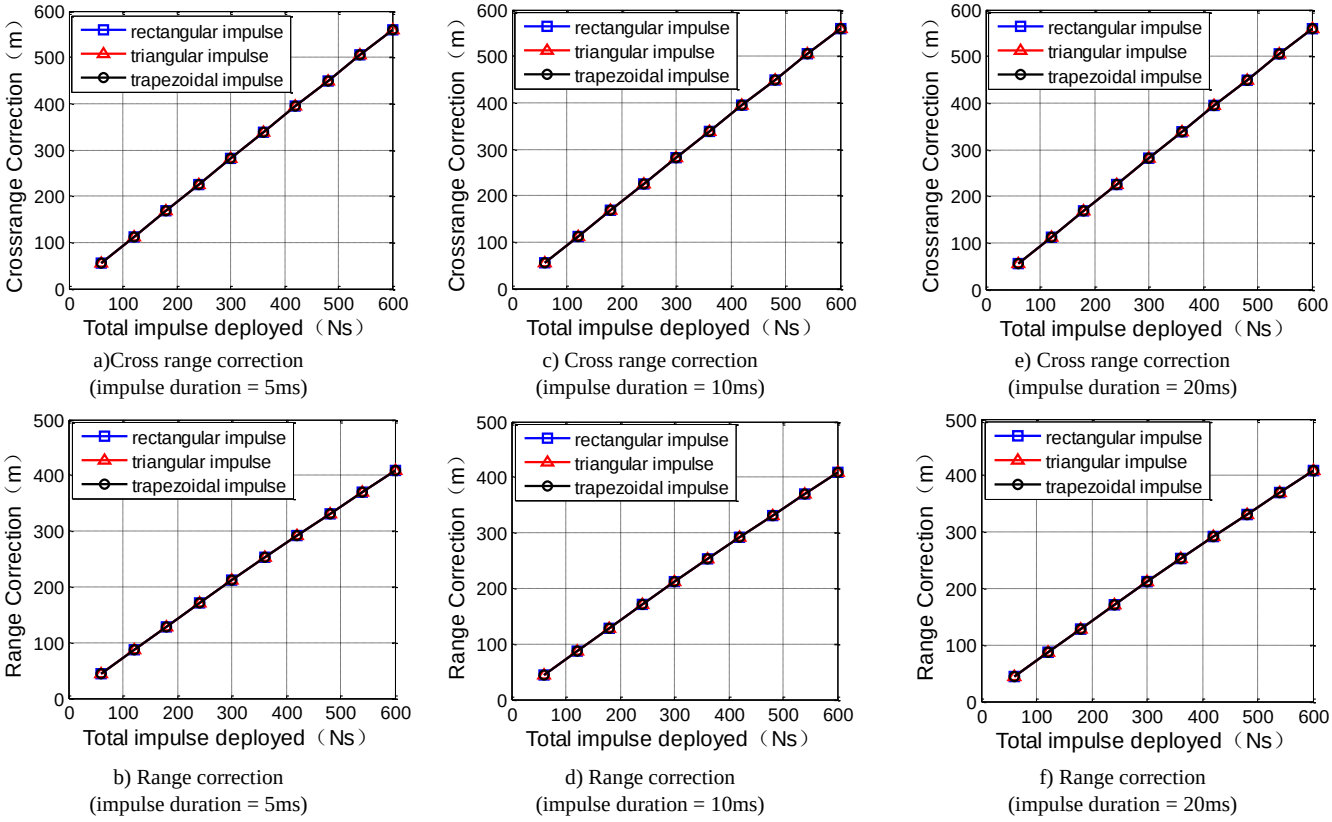

a)Cross range correction (impulse duration = 5ms)

c) Cross range correction (impulse duration = 10ms)

e) Cross range correction (impulse duration = 20ms)

b) Range correction (impulse duration = 5ms)

d) Range correction (impulse duration = 10ms)

f) Range correction (impulse duration = 20ms)

Fig. 5. The impact of parameters of thrusters on correction capability

Fig. 5(a) and Fig. 5(b) consider thrusters with 5 ms impulse duration, while Fig. 5(c) and Fig. 5(d) consider 10 ms impulse duration, and Fig. 5(e) and Fig. 5(f) consider thrusters with 20 ms impulse duration. In all cases, as the results indicated, the trajectory correction capability has a linear relation with the total impulse deployed, and the trajectory correction capability increases steadily as the total impulse increases, however, the trajectory correction capability has little relationship with impulse shapes, max lateral forces, or impulse durations. Therefore, (12) can be obtained by defining the coefficient k as the ratio between the trajectory correction capability R and the total impulse I .

$$R = k \cdot I \tag{12}$$

where k is the coefficient of converting the impulse to the trajectory correction capability, and the coefficient value reflects the correction efficiency of the impulse thruster.

As shown in Fig. 5(a) and Fig. 5(b), correction efficiency of the impulse thruster for range and cross range correction is different, for example, the cross range correction capability is 290m when the total impulse deployed is 300 Ns, whereas the range correction capability is 210m when the total impulse deployed is 300 Ns. The converting coefficients for range and cross range correction, denoted by k_x and k_z respectively, have different values, and it should be noted that the k_x and k_z will change with flight time. Simulation results of k_x and k_z of the rocket are shown in Fig.6. The launch angle of the rocket is 45 deg in the simulations.

As shown in Fig. 6, k_x and k_z have different change trends, k_x increases gradually in ballistic ascending segment and decreases gradually in ballistic descending segment, while k_z decreases gradually with the decrease of time to go. The change trends of k_x and k_z indicate that the longitudinal correction efficiency of impulse thrusters is lower compared to the horizontal correction efficiency in ballistic ascending segment, and longitudinal and horizontal correction efficiency reduces with the decrease of time to go in ballistic descending segment. The change trends of k_x and k_z is import for the design of trajectory correction scheme, which suggests that the impulse thrusters should be fired at time when the correction efficiency is higher to get the maximum trajectory correction capability.

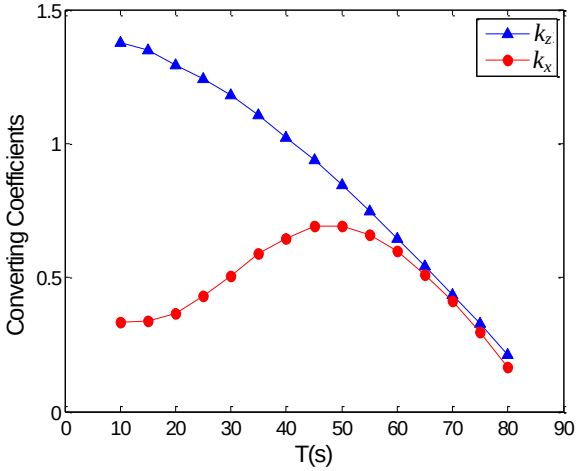

Fig. 6. Converting coefficients vs. flight time

IV. Impulse Utilization Efficiency Analysis

The fin-stabilized projectiles usually spin slowly during the flight time, then the firing delay t_d and the impulse duration t_p have an important impact on the trajectory correction

performance, because they make the actual direction of impulse force has an angle error θ_d with the commanded direction of impulse force, as shown in Fig. 7.

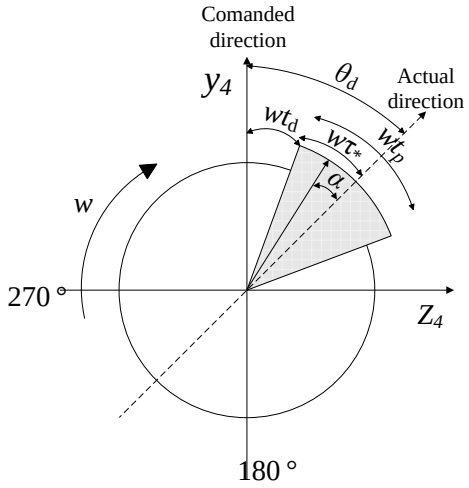

Fig. 7. Firing progress of an impulse thruster

We obtain the expression of θ_d by using I^* depicts the impulse of a thruster, and τ_* depicts the time corresponding to $\frac{1}{2}I^*$:

$$\theta_d = w(t_d + \tau_*) \tag{13}$$

Then the impulse utilization efficiency of an impulse thruster is described as

$$\eta_1 = \frac{I^* \cos(\theta_d)}{I^*} = \cos(wt_d + w\tau_*) \tag{14}$$

The impulse utilization efficiency η_1 can be improved significantly by sending ignition signal of impulse thrusters ahead with the time $t_d + \tau_*$.

At the same time, the thrusters exerted impulse forces and moments over a roll window (denoted as wt_p) of the entire roll cycle, due to the gyroscopic action, as shown in Fig. 7, which will also cause the impulse utilization efficiency loss of thrusters. The impulse utilization efficiency model due to impulse duration of the impulse thrusters with rectangular impulse, triangular impulse, and trapezoidal impulse will be analyzed in the following sections.

A. Rectangular Impulse

For the thrusters with rectangular impulse, the total impulse of a thruster is computed as

$$I^* = \int_0^{t_p} F dt = F_m \tau \tag{15}$$

τ_* is described as

$$\tau_* = \tau / 2 \tag{16}$$

As shown in Fig. 7, α depicts the angle between the direction of impulse force and the actual direction of impulse force during the impulse thruster burns, α is computed according to

$$\alpha = w\tau_* - wt \tag{17}$$

The impulse of a thruster converts to the actual direction is described as

$$I = \int_0^{t_p} F \cos(\alpha) dt \tag{18}$$

Substituting (17) into (18), we obtain

$$I = \int_0^{\tau} F_m \cos(w\tau_* - wt) dt = 2F_m \sin(\frac{w\tau}{2}) / w \tag{19}$$

With the expression of I in (19) and the expression of I^* in (15), the impulse utilization efficiency of the rectangular impulse is computed as

$$\eta_{rec} = I / I^* = \frac{2\sin(\frac{w\tau}{2})}{w\tau} \tag{20}$$

B. Triangular Impulse

For the thrusters with triangular impulse, the total impulse of a thruster is computed as

$$I^* = 2\int_0^{\tau} F dt = \frac{1}{2} F_m (\tau_1 + \tau_2) \tag{21}$$

When $\tau_1 \le \tau_2$, τ_* obeys the following relation:

$$\frac{1}{2}\tau_* \cdot \frac{\tau_*}{\tau_1} F_m = \frac{1}{2} I^* \tag{22}$$

The solution to (22) is:

$$\tau_* = \sqrt{\frac{1}{2}(\tau_1 + \tau_2)\tau_1} \tag{23}$$

When $\tau_1 > \tau_2$, τ_* obeys the following relation:

$$\frac{1}{2}(\tau_1 + \tau_2 - \tau_*) \cdot \frac{(\tau_1 + \tau_2 - \tau_*)}{\tau_2} F_m = \frac{1}{2} I^* \tag{24}$$

The solution to (24) is:

$$\tau_* = \tau_1 + \tau_2 - \sqrt{\frac{1}{2}(\tau_1 + \tau_2)\tau_2} \tag{25}$$

The impulse of a thruster converts to the actual direction is described as:

$$I = \int_0^{\tau_1} F \cos(\alpha) dt + \int_{\tau_1}^{t_p} F \cos(\alpha) dt \tag{26}$$

We obtain (27) by substituting (17) into (26):

$$I = \frac{F_m}{w^2}\left[\frac{\cos(w\tau_* - w\tau_1) - \cos(w\tau_*)}{\tau_1} + \frac{\cos(w\tau_* - w\tau_1) - \cos(w\tau_* - wt_p)}{\tau_2}\right] \tag{27}$$

The impulse utilization efficiency of the triangular impulse is computed as

$$\eta_{tri} = I / I^* = \frac{2}{w^2}\left[\frac{\cos(w\tau_* - w\tau_1) - \cos(w\tau_*)}{\tau_1(\tau_1 + \tau_2)} + \frac{\cos(w\tau_* - w\tau_1) - \cos(w\tau_* - wt_p)}{\tau_2(\tau_1 + \tau_2)}\right] \tag{28}$$

C. Trapezoidal Impulse

For the thrusters with trapezoidal impulse, the total impulse of a thruster can be computed as

$$I^* = \int_0^{t_p} F dt = \frac{F_m}{2}(\tau_1 + 2\tau_2 + \tau_3) \tag{29}$$

τ_* obeys the following relation:

$$\frac{1}{2}F_m\tau_1 + F_m(\tau_* - \tau_1) = \frac{1}{2}(\frac{1}{2}F_m\tau_1 + F_m\tau_2 + \frac{1}{2}F_m\tau_3) \tag{30}$$

The solution to (30) is:

$$\tau_* = \frac{3\tau_1 + 2\tau_2 + \tau_3}{4} \tag{31}$$

The impulse of a thruster converts to the actual direction is described as

$$\begin{aligned} I &= \int_0^{\tau_1} F_m \frac{t}{\tau_1}\cos(\alpha)dt + \int_{\tau_1}^{\tau_1+\tau_2} F_m\cos(\alpha)dt + \int_{\tau_1+\tau_2}^{t_p} \frac{F_m}{\tau_3}(t_p - t)\cos(\alpha)dt \\ &= \frac{F_m}{w^2\tau_1}\left[\cos(w\tau_1 - w\tau_*) - \cos(w\tau_*)\right] \\ &+ \frac{F_m}{w^2\tau_3}\left[\cos(w\tau_1 + w\tau_2 - w\tau_*) - \cos(wt_p - w\tau_*)\right] \end{aligned} \tag{32}$$

The impulse utilization efficiency of the trapezoidal impulse is computed as

$$\begin{aligned} \eta_{tra} = I / I^* = \frac{2}{w^2}\Bigg[&\frac{\cos(w\tau_1 - w\tau_*) - \cos(w\tau_*)}{\tau_1(\tau_1 + 2\tau_2 + \tau_3)} \\ &+ \frac{\cos(w\tau_1 + w\tau_2 - w\tau_*) - \cos(wt_p - w\tau_*)}{\tau_3(\tau_1 + 2\tau_2 + \tau_3)}\Bigg] \end{aligned} \tag{33}$$

Through analyses above, the total impulse utilization efficiency of the thruster with rectangular impulse is computed as

$$\eta = \eta_1 \cdot \eta_{rec} = \frac{2\sin(\frac{w\tau}{2})}{w\tau}\cos(wt_d + w\tau_*) \tag{34}$$

The total impulse utilization efficiency of the thruster with triangular impulse is computed as

$$\begin{aligned} \eta = \eta_1 \cdot \eta_{tri} = \frac{2}{w^2}\Bigg[&\frac{\cos(w\tau_* - w\tau_1) - \cos(w\tau_*)}{\tau_1(\tau_1 + \tau_2)} \\ &+ \frac{\cos(w\tau_* - w\tau_1) - \cos(w\tau_* - wt_p)}{\tau_2(\tau_1 + \tau_2)}\Bigg]\cos(wt_d + w\tau_*) \end{aligned} \tag{35}$$

The total impulse utilization efficiency of the thruster with trapezoidal impulse is computed as

$$\begin{aligned} \eta = \eta_1 \cdot \eta_{tra} = \frac{2}{w^2}\Bigg[&\frac{\cos(w\tau_1 - w\tau_*) - \cos(w\tau_*)}{\tau_1(\tau_1 + 2\tau_2 + \tau_3)} \\ &+ \frac{\cos(w\tau_1 + w\tau_2 - w\tau_*) - \cos(wt_p - w\tau_*)}{\tau_3(\tau_1 + 2\tau_2 + \tau_3)}\Bigg]\cos(wt_d + w\tau_*) \end{aligned} \tag{36}$$

Based on analyses above, the correction capability formula in (12) is rewritten as

$$R = k \cdot \eta \cdot I \tag{37}$$

where R is the trajectory correction capability, I is the total impulse of the thrusters, η is the total impulse utilization efficiency, k is the converting coefficient.

V. Experiments and Discussion

A live firing experiment has been done to investigate the correction performance of impulse thrusters and verify the effectiveness of the trajectory correction capability model. The characters of the rocket has been launched is same to the rocket described in the simulations above. The thruster ring contains 48 impulse thrusters, and each thruster has an impulse of 10.89 Ns. The thruster impulse was modeled as a triangular impulse (F_m=1361 N, τ_1 =2 ms, τ_2 =14 ms) according to its characters, as shown in Fig. 8. The rocket was launched at 200 m above sea level toward a target on the ground with cross range equal zero at a range of 30 km, and the thrusters was designed to correct horizontal impact point deviation of the rocket with the firing interval equals 0.3 s. The trajectory correction start time was set as 20 s. The thruster ignition signal was send ahead with the time $t_d + \tau_*$ to avoid the impulse utilization efficiency loss caused by impulse delay, where τ_* was calculated by (23), and t_d has been measured by professional equipment.

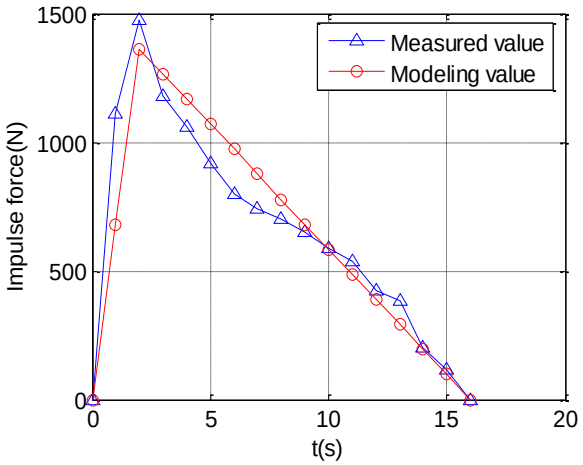

Fig. 8. Impulse model

Fig. 9 shows the changing of the rocket spin rate. The rocket spin rate gets its max value 17.25 r/s at 3.7 s, then reduces gradually and remains smaller than 10 r/s after 20 s. A relatively low spin rate leads to a higher impulse utilization efficiency.

Fig. 10 plots the predicted impact point deviation of the rocket and impulse thrusters fired flags. The predict algorithm of impact point deviation based on perturbation theory has high precision, so it was used to calculate the actual correction distance of thrusters. It can be known from Fig.10 that the horizontal impact point deviation reduces quickly from -813.2 m at 20.05 s to -214.9 m at 35.25 s under the effect of thrusters, so the actual correction distance is 598.3 m.

Table I presents the calculation progress of trajectory correction capability with the correction capability model. As shown in Table I, 48 thrusters were fired during 20.05 s ~ 35.25 s. The converting coefficient k between the thruster impulse and trajectory correction capability was obtained through two-dimensional interpolation, which reduces gradually as the fired time increases, as shown in Fig. 6. The rocket spin rate reduces gradually from 9.75 r/s to 6.66 r/s during the thrusters firing period, corresponding to which the impulse utilization efficiency calculated according to (35) increases gradually from 0.976 to 0.989. The high impulse utilization efficiency benefits from the contributions of relatively low rocket spin rate and short impulse duration. The cross range correction capability of an individual thruster is calculated by its impulse I, converting coefficient k, and impulse utilization efficiency η, according to (37).

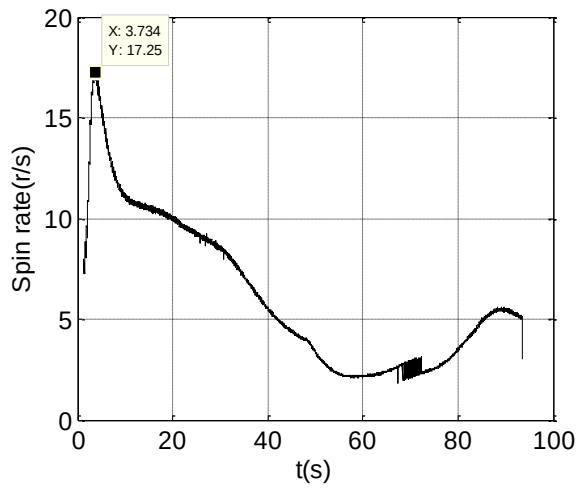

Fig. 9. Rocket spin rate vs. flight time

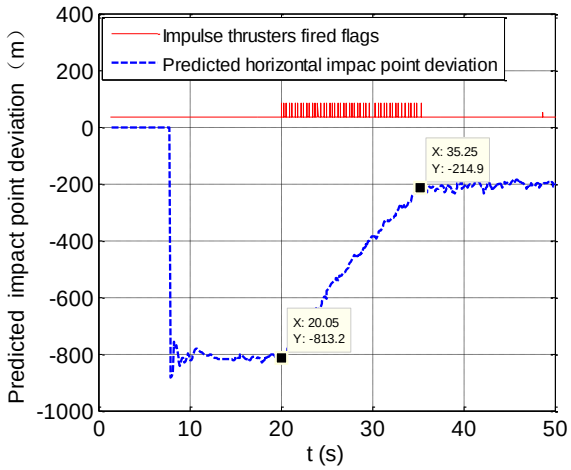

Fig. 10. Horizontal impact point deviation

It can be known from Table I that the individual cross range correction capability reduces gradually as the fired time increases, although the impulse utilization efficiency increases gradually in this period. The reason of this phenomena is that the reduce the change of impulse utilization efficiency is relatively small compared to the change of converting coefficient. Total cross range correction value of 48 impulse thrusters calculated by the trajectory correction capability model is 619.1 m, so the error between the trajectory correction value calculated by trajectory correction capability model and the actual correction distance is 20.8 m, and the ratio between this error and the actual correction distance is 3.4%.

In summary, the trajectory correction capability of impulse thrusters can be calculated by the trajectory correction capability model through modeling the thruster impulse as a rectangular impulse, triangular impulse, or trapezoidal impulse, determining the firing time of thrusters, and measuring the rocket spin rate. The small error between trajectory correction value calculated by the trajectory correction capability model and actual correction distance indicates that the simulation and formulation are effective for engineering design of trajectory correction projectiles with impulse thrusters. To get the demanded trajectory correction capability, the rocket spin rate or thruster impulse duration should be minimized to improve the impulse utilization efficiency, while the impulse thrusters should be designed to be ignited at time when the converting coefficient is higher, and enough impulse thrusters should be deployed according to the quantification of the demanded trajectory correction capability.

TABLE I
CALCULATING OF TRAJECTORY CORRECTION CAPABILITY

No.	Fired time (s)	spin rate (r/s)	k (m/Ns)	η	Correction capability (m)
1	20.01	9.75	1.294	0.976	13.75
2	20.31	9.57	1.291	0.977	13.73
3	20.62	9.57	1.287	0.977	13.69
4	20.93	9.56	1.284	0.977	13.66
5	21.24	9.49	1.281	0.977	13.63
6	21.55	9.52	1.278	0.977	13.59
7	21.85	9.46	1.274	0.977	13.56
8	22.17	9.29	1.271	0.978	13.53
9	22.49	9.35	1.267	0.978	13.49
10	22.81	9.30	1.264	0.978	13.46
11	23.12	9.35	1.261	0.978	13.42
12	23.43	9.30	1.257	0.978	13.39
13	23.74	9.22	1.254	0.978	13.36
14	24.05	8.98	1.251	0.979	13.34
15	24.37	9.15	1.247	0.979	13.29
16	24.69	8.90	1.244	0.980	13.27
17	25.01	8.82	1.240	0.980	13.24
18	25.32	8.88	1.237	0.980	13.20
19	25.63	8.89	1.233	0.980	13.16
20	25.93	8.87	1.229	0.980	13.12
21	26.25	8.72	1.226	0.981	13.09
22	26.55	8.70	1.222	0.981	13.05
23	26.86	8.66	1.218	0.981	13.01
24	27.17	8.60	1.214	0.981	12.97
25	27.48	8.52	1.211	0.981	12.94
26	27.79	8.61	1.207	0.981	12.89
27	28.10	8.54	1.203	0.981	12.86
28	28.41	8.49	1.200	0.981	12.82
29	28.72	8.49	1.196	0.981	12.78
30	29.03	8.40	1.192	0.982	12.75
31	29.35	8.41	1.188	0.982	12.71
32	29.66	8.33	1.185	0.982	12.67
33	30.35	8.24	1.175	0.982	12.58
34	30.65	8.07	1.171	0.983	12.54
35	30.97	7.98	1.166	0.984	12.49
36	31.28	8.01	1.162	0.983	12.44
37	31.60	7.89	1.157	0.984	12.40
38	31.91	7.82	1.152	0.984	12.35
39	32.22	7.65	1.148	0.985	12.31
40	32.56	7.65	1.143	0.985	12.25
41	32.87	7.44	1.138	0.986	12.22
42	33.21	7.41	1.133	0.986	12.16
43	33.57	7.27	1.128	0.986	12.11
44	33.93	7.20	1.122	0.987	12.06
45	34.29	7.14	1.117	0.987	12.01
46	34.60	6.89	1.113	0.988	11.97
47	34.91	6.87	1.108	0.988	11.92
48	35.35	6.66	1.101	0.989	11.85

VI. Conclusion

Trajectory correction capability simulations indicate that the trajectory correction capability has a linear relationship with the total impulse deployed, steadily increases as the impulse is increased, but has little relation with impulse shapes, max lateral forces, or impulse durations.

The actual trajectory correction capability is degraded because projectiles spin and thrusters act with a short-time delay and a certain duration. The relationship between impulse utilization efficiency with impulse duration, projectile spin rate and impulse delay is formulated, taking rectangular impulse, triangular impulse, trapezoidal impulse as examples. A live experiment has been done to investigate the correction performance of impulse thrusters and verify the effectiveness of the trajectory correction capability mode. The experiment result shows that the error between the trajectory correction value calculated by trajectory correction capability model and actual correction distance is 3.4%, which indicates that the simulation and formulation in this paper are effective for engineering design of trajectory correction projectiles with impulse thrusters.

References

[1] T. Harkins and T. Brown, "Using Active Damping as a Precision-Enhancing Technology for 2.75-inch Rockets," *ARL-TR-1772*, U.S. Army Research Laboratory, Aberdeen Proving Ground, MD, 1999.

[2] T. Jitpraphai and M. Costello, "Dispersion Reduction of a Direct Fire Rocket Using Lateral Pulse Jets," *Journal of Spacecraft and Rockets*, Vol.38, No.6, 2001, pp.929-936.

[3] S. K. Gupta, S. Saxena, A. Singhal, and A. K. Ghosh, "Trajectory Correction Flight Control System using Pulsejet on an Artillery Rocket," *Defence Science Journa*l, Vol. 58, No. 1, January 2008, pp. 15-33.

[4] D. Corriveau, C. Berner, and V. Fleck, "Trajectory correction using impulse thrusters for conventional artillery projectiles," *23RD International Symposium on Ballistics Tarragona*, Spain, 16-20 April, 2007.

[5] D. Corriveau, P. Wey, and C. Berner, "Analytical Model Development and Impulse Thrusters Pairing Guidelines for Trajectory Corrections of Fin-stabilized Projectiles," *48th AIAA Aerospace Sciences Meeting Including the New Horizons Forum and Aerospace Exposition*, 4-7 January 2010, Orlando, Florida.

[6] B. Pavković and M. Pavić, "Frequency-Modulated Pulse-Jet Control of an Artillery Rocket," *Journal of Spacecraft and Rockets*, Vol. 49, No. 2, 2012.

[7] Min Gao, Yongwei Zhang, and Suochang Yang, "Firing Control Optimization of Impulse Thrusters for Trajectory Correction Projectiles," *International Journal of Aerospace Engineering*, vol. 2015, Article ID 781472, 11 pages, 2015. doi:10.1155/2015/781472